

# We are IntechOpen, the world's leading publisher of Open Access books Built by scientists, for scientists

6,900

Open access books available

186,000

International authors and editors

200M

Downloads

Our authors are among the

154

Countries delivered to

TOP 1%

most cited scientists

12.2%

Contributors from top 500 universities



WEB OF SCIENCE™

Selection of our books indexed in the Book Citation Index  
in Web of Science™ Core Collection (BKCI)

Interested in publishing with us?  
Contact [book.department@intechopen.com](mailto:book.department@intechopen.com)

Numbers displayed above are based on latest data collected.  
For more information visit [www.intechopen.com](http://www.intechopen.com)



---

# Thermodynamic Activity-Based Michaelis Constants

---

Anton Wangler, Mark Jonathan Bunse,  
Gabriele Sadowski and Christoph Held

Additional information is available at the end of the chapter

<http://dx.doi.org/10.5772/intechopen.80235>

---

## Abstract

The classical approach towards analysing the influence of co-solvents (i.e., cellular molecules that are chemically inert and do not act as reacting agents) on the Michaelis constants of enzyme-catalysed reactions is empirical. More precisely, reaction kinetics is usually mathematically modelled by fitting empirical parameters to experimental concentration vs. time data. In this chapter, a thermodynamic approach is presented that replaces substrate concentrations by thermodynamic activities of the substrates. This approach allows determining activity-based Michaelis constants. The advantage of such activity-based constants  $K_M^a$  over their concentration-based counterparts  $K_M^{obs}$  is twofold: First,  $K_M^a$  is independent of any co-solvent added (while  $K_M^{obs}$  is not) as long as it does not directly interfere with the reaction mechanism (e.g., inhibitor or activator). Second, known  $K_M^a$  values allow predictions of Michaelis constants for different enzymes and reactions under co-solvent influence. This is demonstrated for a pseudo-one-substrate peptide hydrolysis reaction as well as for more complex two-substrate alcohol dehydrogenase reactions.

**Keywords:** enzyme kinetics, thermodynamics, activity coefficient, co-solvent, ePC-SAFT

---

## 1. Introduction

Understanding the kinetics of enzyme-catalysed reactions is a key aspect not just in the field of biology but also of high relevance for biocatalysis in the industry as enzymes are highly suitable for the production of fine chemicals [1]. The advantage of enzyme catalysis is that high enantioselectivity [2, 3] can often be realised under mild reaction conditions (ambient temperature and pressure).

Key properties for the study of enzyme-catalysed reactions are reaction yield and reaction kinetics. In case of the reaction yield, thermodynamic states an independence of the

equilibrium position from the catalyst involved (as long as the catalyst concentration is low) [4–7]. In contrast, reaction kinetics strongly depends on the catalyst [8, 9]. This means that different enzymes used for the same reaction will cause different kinetic profiles for the considered reaction; this is represented by the experimental (concentration-based) Michaelis constant  $K_M^{obs}$  and the catalytic constant  $k_{cat}$ . These constants are thus enzyme-specific. Even more, the presence of co-solvents (i.e., chemically inert substances that do not act as metabolites) such as organic and inorganic compounds, salts and polymers might significantly influence such kinetic constants. In literature, the influence of diverse co-solvents on kinetics of a large amount of different enzyme-catalysed reactions is reported [7, 10–13]. It is common practice to empirically describe the co-solvent effects on the kinetic parameters; this requires a co-solvent-dependent consideration of enzyme kinetics. Further, it is discussed whether co-solvent-induced changes on  $K_M^{obs}$  are directly related to interactions between co-solvent and the catalytic centre or other parts of the enzyme. These former accepted relations have been recently revised in the publications of Grosch et al. [10], Pleiss [14, 15] and Wangler et al. [7]. These recent works suggested an approach, which is independent of the enzyme itself. In their approach,  $K_M^{obs}$  is influenced by co-solvent-substrate interactions caused by co-solvent-induced non-covalent molecular interactions between substrate and reaction medium, which the co-solvent is part of. By changing the perspective from co-solvent-enzyme interactions to co-solvent-substrate interactions, a new activity-based Michaelis constant  $K_M^a$  was proposed, which is based on thermodynamic activities of the substrates under co-solvent influence. The advantage of this treatment is that  $K_M^a$  is independent of any kind or concentration of co-solvents present in the reaction mixture. This is even more impressive as these recent works neglect co-solvent-enzyme interactions in order to obtain co-solvent independent values for  $K_M^a$ . Further, the advantage of such activity-based treatment over the concentration-based approach is to establish a non-empirical method towards predicting and understanding co-solvent effects on the Michaelis constants without the need of experimental kinetic data of reaction mixtures containing co-solvents. This method requires activity coefficients  $\gamma$  of the substrates. These activity coefficients describe the molecular interactions in the reaction mixture, and they can be predicted with different thermodynamic models, e.g., NRTL [16], UNIFAC [17] or ePC-SAFT [18].

In this chapter, an approach is presented to determine  $K_M^a$  values based on  $K_M^{obs}$  values of the neat (co-solvent-free) reaction system and the activity coefficients of the substrates. The considered reactions are the hydrolysis of N-succinyl-L-phenylalanine-p-nitroanilide (SPNA) catalysed by the enzyme  $\alpha$ -chymotrypsin ( $\alpha$ -CT) and a two-substrate reaction, namely the reduction of acetophenone (ACP) catalysed by alcohol dehydrogenase 270 (ADH 270) and by alcohol dehydrogenase 200 (ADH 200). Determined  $K_M^a$  values under neat conditions were used to predict the co-solvent influence on  $K_M^{obs}$  values of the reactions under consideration. These predicted values were finally compared to experimental data to validate this approach.

## 2. Pseudo-one-substrate reactions

### 2.1. Theoretical background

#### 2.1.1. Concentration-based approach

Examples for one-substrate reactions are isomerase reactions where one substrate is converted to another without any change to the chemical composition of the molecule. Examples can be found in glycolysis, one being the reversible conversion of 3-phosphoglycerate (substrate  $S$ ) to 2-phosphoglycerate (product  $P$ ) catalysed by phosphoglycerate mutase (enzyme  $E$ ). The general reaction scheme of a one-substrate reaction is given in Eq. (1).



The kinetics of the reaction according to Eq. (2) is commonly described by the Michaelis-Menten equation including the reaction rate  $v$ , the maximum reaction rate  $v_{max}$ , the Michaelis constant  $K_M^{obs}$  and the substrate molality  $m_S$  in mol/kg<sub>water</sub>.

$$v = \frac{v_{max} \cdot m_S}{K_M^{obs} + m_S} \quad (2)$$

Eq. (2) is visualised exemplary by plotting of  $v$  over  $m_S$  in **Figure 1**.

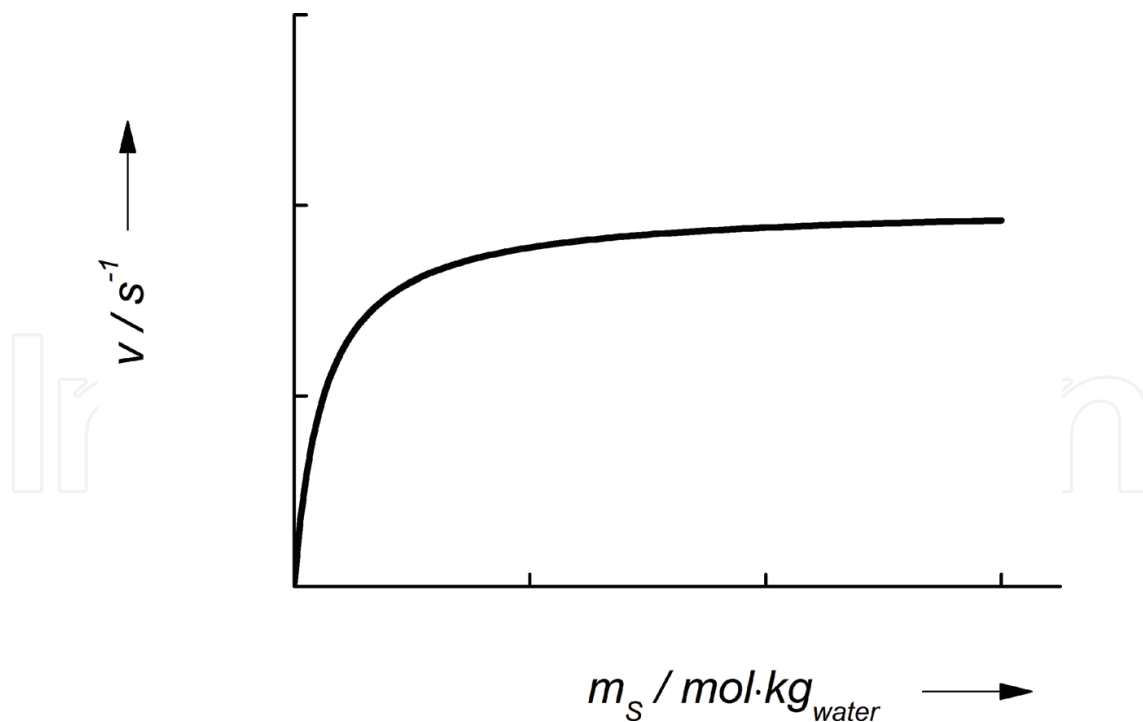
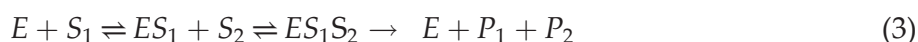


**Figure 1.** Qualitative Michaelis-Menten plot of the reaction rate  $v$  plotted over the substrate molality  $m_S$  according to Eq. (2).

As can be seen from Eq. (2) and **Figure 1**, the reaction rate follows a hyperbolic curve over increasing substrate concentrations. Further,  $K_M^{obs}$  defines the shape of the curve as it is the concentration of substrate at which the reaction velocity becomes half of its maximal value  $0.5 v_{max}$ . Based on this, the importance of  $K_M^{obs}$  becomes obvious. If the value of  $K_M^{obs}$  is low compared to  $m_S$  required to reach  $v = v_{max}$ , it can be deduced that the cellular concentration of the substrates will also be close to  $K_M^{obs}$  as a significant increase in  $m_S$  (e.g., fivefold) will never increase  $v$  more than by a factor of 2 [9]. Thus, the knowledge of  $K_M^{obs}$  is of high importance for biology and for technical applications of enzyme-catalysed reactions.

Unfortunately, the majority of enzyme-catalysed reactions are not one-substrate reactions; in such cases, the reaction scheme increases in complexity. However, it is often still possible to apply pseudo-one-substrate reaction conditions given that the molality of one substrate is much higher than the molality required to obtain  $v_{max}$ . These conditions are obtained if substrate simultaneously presents the reaction solvent, which is the case for hydrolysis reactions. A general scheme for a two-substrate reaction is given in Eq. (3).



In Eq. (3), substrates are labelled as  $S_1$  and  $S_2$ ; the reaction mechanism (ordered or random) shall not be discussed at this point. In this case, the Michaelis-Menten equation changes to Eq. (4), which contains the Michaelis constants for substrate 1  $K_{MS1}^{obs}$  and substrate 2  $K_{MS2}^{obs}$  as well as the inhibition constant  $K_{iS1}^{obs}$ , which defines the reaction mechanism [8, 9].

$$v = \frac{v_{max} \cdot m_{S1} \cdot m_{S2}}{K_{iS1}^{obs} \cdot K_{MS2}^{obs} + K_{MS1}^{obs} \cdot m_{S2} + K_{MS2}^{obs} \cdot m_{S1} + m_{S1} \cdot m_{S2}} \quad (4)$$

In the case of a hydrolysis reaction taking place in water as reaction solvent, the molality of substrate 2  $m_{S2}$  (water) is usually two to three orders of magnitude higher than the molality of substrate 1, which gets cleaved by the enzyme. Rearranging Eq. (4) leads back to the Michaelis-Menten equation under this assumption shown in Eqs. (5)–(7).

$$v = \frac{v_{max} \cdot m_{S1}}{\frac{(K_{iS1}^{obs} \cdot K_{MS2}^{obs})}{m_{S2}} + K_{MS1}^{obs} + K_{MS2}^{obs} \cdot \frac{m_{S1}}{m_{S2}} + m_{S1}} \quad (5)$$

$$m_{S1} \gg m_{S2} \text{ and } m_{S1} \gg K_{iS1}^{obs} \cdot K_{MS2}^{obs} \quad (6)$$

$$v = \frac{v_{max} \cdot m_{S1}}{K_{M1}^{obs} + m_{S1}} \quad (7)$$

To be able to compare reactions from different research groups and further for different enzymes catalysing the same reaction, the Michaelis-Menten equation has to be normalised to the total enzyme concentration  $m_E$  according to Eq. (8).

$$\frac{d \frac{m_P}{m_E}}{dt} = \frac{dm_P}{dt} \cdot \frac{1}{m_E} = v' = \frac{k_{cat} \cdot m_S}{K_M^{obs} + m_S} \quad (8)$$

The determination of  $k_{cat}$  and  $K_M^{obs}$  is usually performed by measuring reaction rates for different substrate concentrations as shown in **Figure 1**. While this approach is common, it also poses a lot of difficulties and causes high uncertainties. The determination of  $k_{cat}$  requires that the solubility of the substrate has to be higher than the molality  $m_S$  that is required for reaching  $k_{cat}$ . Lowering the enzyme concentration and thus the required molality  $m_S$  often causes diffusion limitations that might lead to highly uncertain kinetic constants. Another possible issue is contrary, as a reaction might require high concentrations of an expensive substrate to determine  $k_{cat}$ . To overcome these possible limitations, the Lineweaver-Burk equation is commonly applied for the determination of the kinetic constants [19].

$$\underbrace{\frac{1}{v'}}_y = \underbrace{\frac{K_M^{obs}}{k_{cat}}}_m \cdot \underbrace{\frac{1}{m_S}}_x + \underbrace{\frac{1}{k_{cat}}}_b \quad (9)$$

Through this linearization, a plot of  $(v')^{-1}$  over  $m_S^{-1}$  yields the kinetic constants: The slope (*Sl*) and the ordinate (*Or*) of the obtained linear fit can be used to determine  $K_M^{obs}$  and  $k_{cat}$  as given in Eqs. (10) and (11).

$$Sl = \frac{K_M^{obs}}{k_{cat}} \quad (10)$$

$$Or = \frac{1}{k_{cat}} \quad (11)$$

### 2.1.2. Activity-based approach

As presented in Section 2.1.1, the Michaelis constant is determined based on the molality  $m_S$ . If co-solvents are added to the neat reaction mixtures, the experimental procedure has to be performed also for the changed conditions. From the perspective of process design, this poses a huge cost-intensive and time-consuming approach towards finding suitable co-solvents for the desired application.

To be able to predict co-solvent influences on pseudo-one-substrate reactions, a thermodynamic co-solvent-independent Michaelis constant, further referred to as  $K_M^a$ , has to be determined.  $K_M^a$  is a constant value, which does not depend on co-solvent given that the co-solvent does not disturb the reaction mechanism (e.g., co-solvent acts as inhibitor or activator) and that the co-solvent has no denaturing effect on the enzyme.  $K_M^a$  can be determined under neat (co-solvent-free) conditions by replacing the molality  $m_S$  in Eq. (9) with thermodynamic activities of the substrate  $a_S$ . The latter are accessible by multiplying the concentration of a substrate by the respective concentration-based activity coefficient (molality-based  $\gamma_S^m$ , mole-fraction-based  $\gamma_S^x$  or molarity-based  $\gamma_S^c$ ) as shown in Eq. (12) [20–22]:

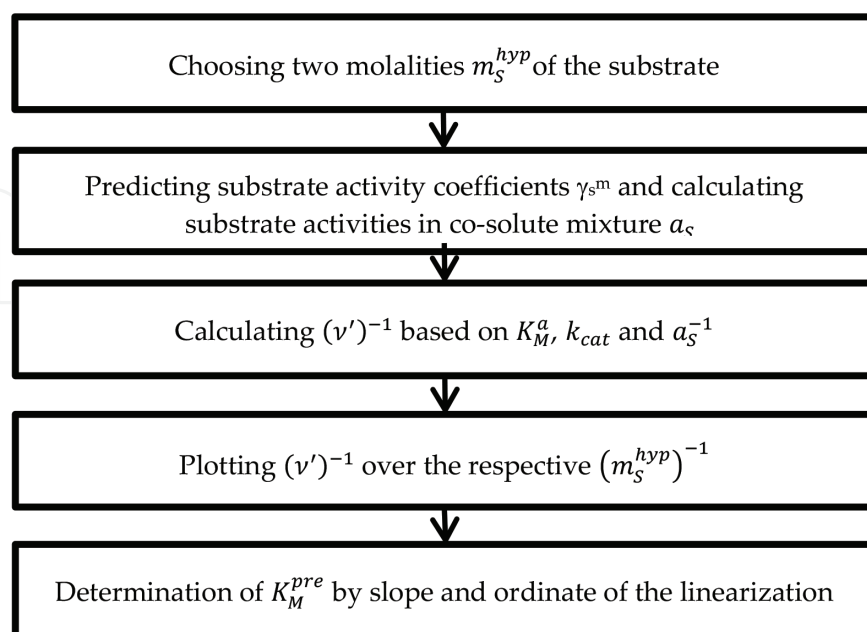
$$a_S[-] = x_S \cdot \gamma_S^x = m_S \cdot \gamma_S^m = c_S \cdot \gamma_S^c \quad (12)$$

In the following, molality-based  $\gamma_S^m$  will be used to analyse the data. Replacing molalities in Eq. (9) with activities leads to an activity-based Lineweaver-Burk equation:

$$\frac{1}{v'} = \frac{K_M^a}{k_{cat}} \cdot \frac{1}{a_S} + \frac{1}{k_{cat}} \quad (13)$$

To determine  $K_M^a$ , the experimental  $(v')^{-1}$  values, which were determined for different  $m_S^{-1}$  values, are further plotted over the reciprocal substrate activity  $a_S^{-1}$ . It is noteworthy that this procedure does not change the value of  $k_{cat}$  [7, 23]. Under the assumption that the addition of a co-solvent only changes non-covalent interactions between the substrate and the other components in the reaction mixture,  $K_M^a$  is assumed to be a constant value. That is, any observed change in  $K_M^{obs}$  is directly reflected in  $\gamma_S^m$ . With this knowledge, a prediction of  $K_M^{obs}$  under co-solvent influence becomes possible. For this, two hypothetical molalities of the substrate  $m_S^{hyp}$  are chosen randomly. Afterwards, activity coefficients of the substrate in the co-solvent system are predicted and the respective activities are calculated. Further, a random value of  $k_{cat}$  (e.g., value of the neat reaction) is chosen. Note that  $k_{cat}$  is a factor that cancels out during the linearization to determine  $K_M^{pre}$  (see Eq. (13)). In the next step, the predicted activities together with  $K_M^a$  and  $k_{cat}$  are used to predict  $(v')^{-1}$  according to Eq. (13). Predicted  $(v')^{-1}$  values are afterwards plotted over the chosen reciprocal molalities  $(m_S^{hyp})^{-1}$ . In the final step, the predicted concentration-based Michaelis constant  $K_M^{pre}$  is determined according to Eq. (9). The process to determine  $K_M^{pre}$  is illustrated in **Scheme 1**.

As can be seen, the major aspect for the prediction of the Michaelis constants is the ability to predict the substrate activity coefficients. For this, a physically sound model, namely the electrolyte perturbed-chain statistical associating fluid theory (ePC-SAFT) was used in this work. This model has already been applied successfully to complex mixtures containing low-soluble molecules [24], PEG and salts [25] and electrolytes [20] while also being applied



**Scheme 1.** Steps for the prediction of the concentration-based Michaelis constant  $K_M^{pre}$  under the influence of co-solvents. Predictions are based on the determined activity-based Michaelis constant  $K_M^a$ .

simultaneously to mixtures with up to eight components [4], and thus, it provides a reliable model basis for this work.

The ePC-SAFT equation of state is based on PC-SAFT, developed and proposed by Gross and Sadowski [26] and extended for electrolyte systems by Cameretti et al. [18] ePC-SAFT provides an expression for the residual Helmholtz energy  $a^{res}$  calculated from different contributions as shown in Eq. (14):

$$a^{res} = a^{hc} + a^{disp} + a^{assoc} + a^{ion} \quad (14)$$

In Eq. (14), the reference system is seen as a chain of hard spheres, which is represented by the contribution  $a^{hc}$ . The perturbations to this hard-chain reference system are accounted for in ePC-SAFT by the molecular dispersive interactions, characterised by the Van der Waals energy incorporated in  $a^{disp}$  and by the associative hydrogen bonding forces represented in  $a^{assoc}$ . As an addition for electrolyte systems, the Coulomb interactions based on the Debye-Hückel equation are expressed by  $a^{ion}$ . Based on  $a^{res}$ , fugacity coefficients  $\varphi$  can be calculated which allow determining the activity coefficients  $\gamma_s^x$  using Eq. (15).

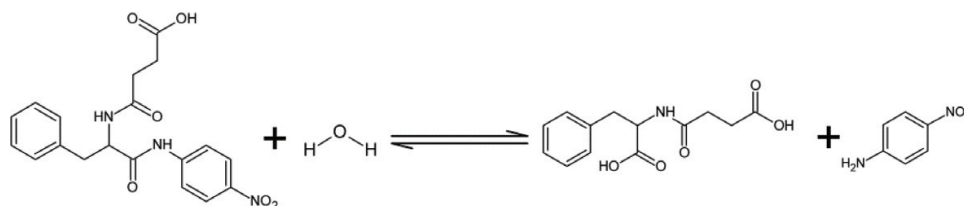
$$\gamma_s^x = \frac{\varphi_i(T, p, \vec{x})}{\varphi_{0i}(T, p, x_i = 1)} \quad (15)$$

In Eq. (15),  $0i$  denotes the pure component, which is the reference state at the same temperature  $T$  and pressure  $p$  as the actual solution of the composition  $\vec{x}$ . This means that activity coefficients can be estimated independent of the amount of components, temperature and pressure of the solution regarded. Eq. (15) is finally used with Eq. (12) to obtain the molality-based  $\gamma_s^m$ .

## 2.2. Kinetic assays

In this work, a pseudo-one-substrate reaction is presented using the hydrolysis of SPNA catalysed by the enzyme  $\alpha$ -CT. The reaction mechanism is given in **Scheme 2**.

The kinetic measurements have been discussed already in [7] and are briefly summarised here. Lyophilized powder of  $\alpha$ -CT was used as catalyst, and trimethylamine N-oxide (TMAO) and urea were used as co-solvents. Measurements were carried out in Tris-HCl buffer (100 mmol/kg<sub>water</sub> tris(hydroxymethyl)aminomethane, pH 8.0). The kinetic measurements of the neat and co-solvent reaction mixtures of the SPNA hydrolysis reactions were performed in a stopped-flow system (HPSF-56 of Hi-Tech Scientific) [27, 28]. In a first step, the substrate stock solution



**Scheme 2.** Reaction scheme for the hydrolysis of SPNA catalysed by  $\alpha$ -chymotrypsin. Products of the hydrolysis reaction are N-(3-carboxypropanoyl)phenylalanine and p-nitroaniline, respectively.

containing SPNA and the respective co-solvent in a 100 mol/kg<sub>water</sub> Tris-HCl buffer at pH 8 and the enzyme stock solution containing the respective co-solvent in a 100 mol/kg<sub>water</sub> Tris-HCl buffer at pH 8 were prepared and loaded for injection in the measurement cell. After simultaneous injection, the measurement cell was constantly monitored for the extinction at 410 nm wavelength, allowing the determination of the time-dependent change in the 4-NA concentration. The pH values of the stock solutions were measured directly before the start of the reaction to ensure no pH effect on  $K_M^{pre}$ ; a pH electrode was used from Mettler Toledo with an uncertainty of  $\pm 0.01$ . The measured systems presented in this work are given in **Table 1**.

### 2.3. Results and discussion

In a first step, the concentration-based Michaelis constant  $K_M^{obs}$  was determined under neat conditions. The respective Lineweaver-Burk plot is given in **Figure 2**.

As can be seen from **Figure 2**, a linear relation between the reciprocal molality of the substrate  $m_{SPNA}^{-1}$  and the reciprocal normalised reaction rate  $(v')^{-1}$  can be observed. This relation allowed the determination of  $K_M^{obs}$ ; as a result, a value of  $1.76 \pm 0.12$  mmol/kg<sub>water</sub> [7] was obtained for the SPNA hydrolysis. The activity-based Michaelis constant  $K_M^a$  was then obtained with activity coefficients of SPNA, which were predicted for each substrate molality with ePC-SAFT. The pure component and binary interaction parameters used for the ePC-SAFT prediction are listed in **Tables 2** and **3**.

Note that in a first step, mole-fraction-based activity coefficients were obtained with ePC-SAFT. Eq. (12) was used to convert these into molality-based activity coefficients; these were used throughout this work. In the next step, a plot of the determined  $(v')^{-1}$  over the predicted reciprocal  $a_{SPNA}^{-1}$  was created. Based on this plot,  $K_M^a$  was determined in analogy to the determination of  $K_M^{obs}$  as shown in **Figure 2**, resulting in a value of  $K_M^a = 0.0686$ . This value was used as input value for the prediction of co-solvent influence on  $K_M^{obs}$  according to **Figure 2**. The comparison between this prediction and the experimental  $K_M^{obs}$  values is shown in **Figure 3** and **Table 4**.

Co-solvent	$m_{co-solvent}$ (mol/kg <sub>water</sub> )	$m_{SPNA}$ (mmol/kg <sub>water</sub> )
Neat	–	0.125–1
TMAO	0.5	0.125–1
Urea	1	0.250–1
DMSO	2.1	0.250–1
DMSO	4.2	0.125–1

Enzyme concentration was 8  $\mu\text{mol}/\text{kg}_{\text{water}}$  in all kinetic assays.

**Table 1.** Overview of the measured systems to determine concentration-based Michaelis constants  $K_M^{obs}$ , adapted from [7], including the co-solvent and its concentration and the initial SPNA concentration range regarded.

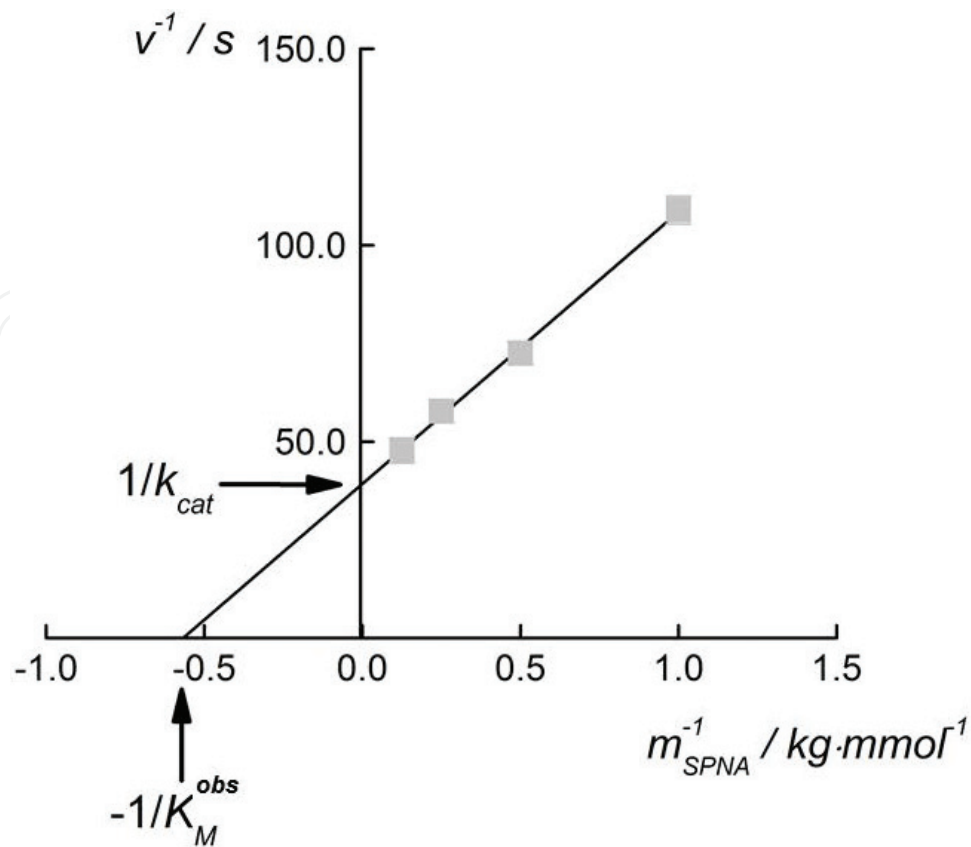


**Figure 2.** Lineweaver-Burk plot for the determination of the concentration-based Michaelis constant of SPNA  $K_M^{obs}$  at  $T = 25^\circ C$ ,  $p = 1$  bar and  $pH = 8$  in Tris-HCl buffer [7]. The plot shows experimental data points of the neat measurements (squares) which are obtained from the inverse turnover frequency  $(v')^{-1}$  over the inverse substrate molality of SPNA  $m_{SPNA}^{-1} \cdot K_M^{obs}$  was obtained by linear regression of the experimental data and extrapolation to the abscissa as shown.

Component	$m_i$ (-)	$\sigma_i$ (Å)	$\frac{u_i}{k_B}$ (K)	$N_i^{assoc}$	$\frac{\epsilon_i B_i}{k_B}$ (K)	$\kappa^{A_i B_i}$ (-)
Water [29]	1.204	[A]	353.95	1:1	2425.7	0.0451
DMSO [29]	2.922	3.28	355.69	1:1	0	0.0451
Urea [29]	4.242	2.45	368.23	1:1	3068.7	0.0010
TMAO [30]	8.93	2.25	245.44	1:1	0	0.0451
SPNA [7]	13.500	4.00	249.95	2:2	4351.0	0.0090

[A]  $\sigma_i = 2.7927 + 10.11 \cdot \exp(-0.01775 \cdot T) - 1.417 \cdot \exp(-0.01146 \cdot T)$ ,  $T$  in Kelvin.

**Table 2.** ePC-SAFT pure-component parameters from [7, 29, 30].

As can be seen in **Figure 3** and **Table 4**, an accurate prediction of the co-solvent-induced changes in  $K_M^{obs}$  is possible. For both DMSO concentrations, predictions are even quantitatively correct within the experimental uncertainties. This is of special importance for the hydrolysis reaction under investigation since DMSO has the strongest impact on  $K_M^{obs}$ . The big advantage of  $K_M^a$  over  $K_M^{obs}$  is that it is a constant value independent of the co-solvent. This fact further

Mixture	$k_{ij}$ (-)
Water-DMSO [30]	-0.065
Water-urea [30]	-0.044
Water-TMAO [30]	-0.149
Water-SPNA [7]	-0.132
DMSO-SPNA [7]	-0.117
Urea-SPNA [7]	-0.203
TMAO-SPNA [7]	-0.220

**Table 3.** ePC-SAFT binary interaction parameters [7, 29, 30].

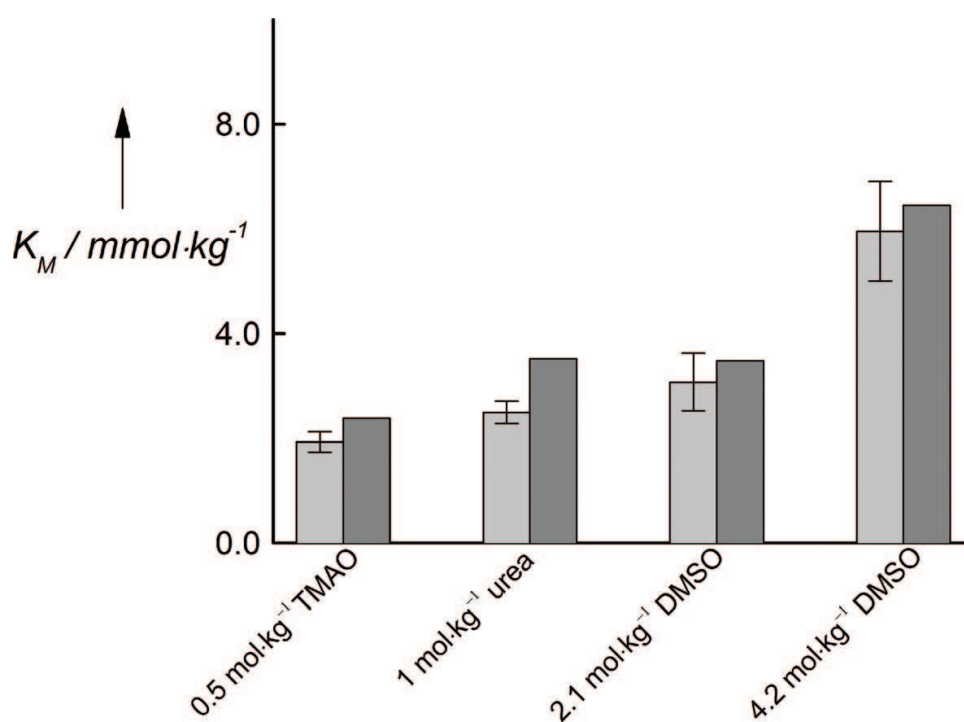


**Figure 3.** Comparison between experimental concentration-based Michaelis constants  $K_M^{obs}$  (light grey bars) at  $T = 25^\circ\text{C}$ ,  $p = 1$  bar and  $\text{pH} = 8$  in Tris-HCl buffer and the predicted Michaelis constants  $K_M^{pre}$  (dark grey bars). For the predictions, a constant  $K_M^a$  value of 0.0686 was used and the activity coefficients were predicted with ePC-SAFT based on the parameters from **Tables 2** and **3**. Reprinted from [7].

allows predicting  $K_M^{obs}$  without the need for additional experimental data. This proves the validity of the proposed modelling approach for pseudo-one-substrate reactions and validates the assumption that co-solvent-substrate interactions are responsible for the dependence of  $K_M^{obs}$  on co-solvents. Thus, this indirectly disproves that enzyme-co-solvent effects are responsible for such changes of  $K_M^{obs}$ . However, as enzyme-catalysed reactions are mostly multi-substrate reactions with two substrates of low concentrations, the following section presents the transfer of the gained insight and methods to two-substrate reactions.

Co-solvent	$m_{co-solvent}$ (mol/kg <sub>water</sub> )	$K_M^{obs}$ (mmol/kg <sub>water</sub> )	$K_M^{pre}$ (mmol/kg <sub>water</sub> )
TMAO	0.5	1.93 ± 0.19	2.38
Urea	1	2.50 ± 0.21	3.51
DMSO	2.8	3.08 ± 0.54	3.48
DMSO	4.2	5.96 ± 0.95	6.45

$K_M^{pre}$  were predicted using  $K_M^a$  determined from experimental  $K_M^{obs} = 1.76 \text{ mmol/kg}_{water}$  of the neat reaction [7].

**Table 4.** Comparison between the experimental  $K_M^{obs}$  with the respective predicted values  $K_M^{pre}$  under the influence of the co-solvents TMAO, urea or DMSO at  $T = 25^\circ\text{C}$ ,  $p = 1 \text{ bar}$  and  $\text{pH} = 8$  in Tris-HCl buffer.

### 3. Two-substrate reactions

#### 3.1. Theoretical background

##### 3.1.1. Concentration-based approach

As presented in Section 2.1.1 ('pseudo') one-substrate reactions occur seldom in enzyme catalysis. Enzyme catalysis often requires co-substrate that is present in a limiting concentration (e.g., NADH, ATP, GTP). A two-substrate reaction can be described by Eq. (16), which cannot be simplified further:

$$v' = \frac{k_{cat} \cdot m_{S1} \cdot m_{S2}}{K_{iS1}^{obs} \cdot K_{MS2}^{obs} + K_{MS1}^{obs} \cdot m_{S2} + K_{MS2}^{obs} \cdot m_{S1} + m_{S1} \cdot m_{S2}} \quad (16)$$

Two-substrate reactions can have a specific binding order attached to them. To account for this, the inhibition constant of S1  $K_{iS1}^{obs}$  based on the Haldane relation was accounted for in this work; if  $K_{iS1}^{obs}$  is lower than  $K_{M,S1}^{obs}$ , an ordered mechanism is present in which S1 has to bind first [8, 31]. The Lineweaver-Burk linearization of Eq. (16) leads to Eq. (17):

$$\underbrace{\frac{1}{v'}}_y = \cdot \underbrace{\left( \frac{K_{iS1}^{obs} \cdot K_{MS2}^{obs}}{k_{cat} \cdot m_{S2}} + \frac{K_{MS1}^{obs}}{k_{cat}} \right)}_m \cdot \underbrace{\frac{1}{m_{S1}}}_x + \underbrace{\left( \frac{K_{MS2}^{obs}}{k_{cat} \cdot m_{S2}} + \frac{1}{k_{cat}} \right)}_b \quad (17)$$

Note that Eq. (17) does not show any direct relation between the Michaelis constants and the ordinate, slope or the abscissa of the linearization. In the case of two-substrate reactions, a two-step linearization process is suggested. For this, the molality of one of the substrates, in this case  $m_{S2}$ , is chosen to be at least 50 times higher than  $m_{S1}$ . Under this assumption, a so-called *primary plot* can be created. For this, different levels of  $m_{S2}$  that are regarded to be constant over the short reaction time are chosen for varying  $m_{S1}$ ; then, a family of straight lines are obtained as shown exemplarily in **Figure 4**.

Each of the straight lines in **Figure 4** has its own slope ( $S_l^{prim}$ ) and ordinate ( $O_r^{prim}$ ); both,  $S_l^{prim}$  and  $O_r^{prim}$  are a function of  $m_{S2}$  as shown in Eqs. (18) and (19).

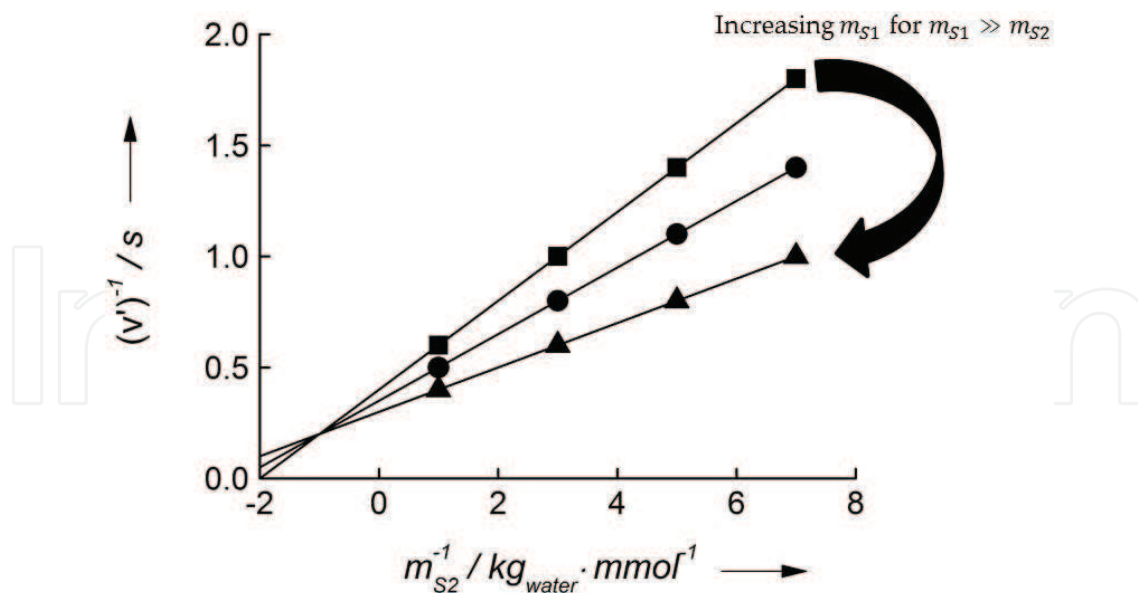


**Figure 4.** Exemplary *primary plot* for a two-substrate reaction obtained from plotting the inverse turnover frequency  $(v')^{-1}$  over the inverse substrate molality of substrate 2  $m_{S2}^{-1}$  for different pseudo-constant molalities of substrate 1  $m_{S1}$ . Molalities  $m_{S1}$  increase in the order of  $m_{S1, \text{squares}} > m_{S1, \text{circles}} > m_{S1, \text{triangles}}$ .

$$SI^{prim} = \frac{K_{iS1}^c \cdot K_{MS2}^c}{k_{cat}} \cdot \frac{1}{m_{S2}} + \frac{K_{MS1}^c}{k_{cat}} \quad (18)$$

$$Or^{prim} = \frac{K_{MS2}^c}{k_{cat}} \cdot \frac{1}{m_{S2}} + \frac{1}{k_{cat}} \quad (19)$$

Eqs. (18) and (19) again show a linear correlation between  $SI^{prim}$  and  $m_{S2}^{-1}$  as well as between  $Or^{prim}$  and  $m_{S2}^{-1}$ , respectively. This allows for another linearization step represented in two *secondary plots* in **Figure 5**.

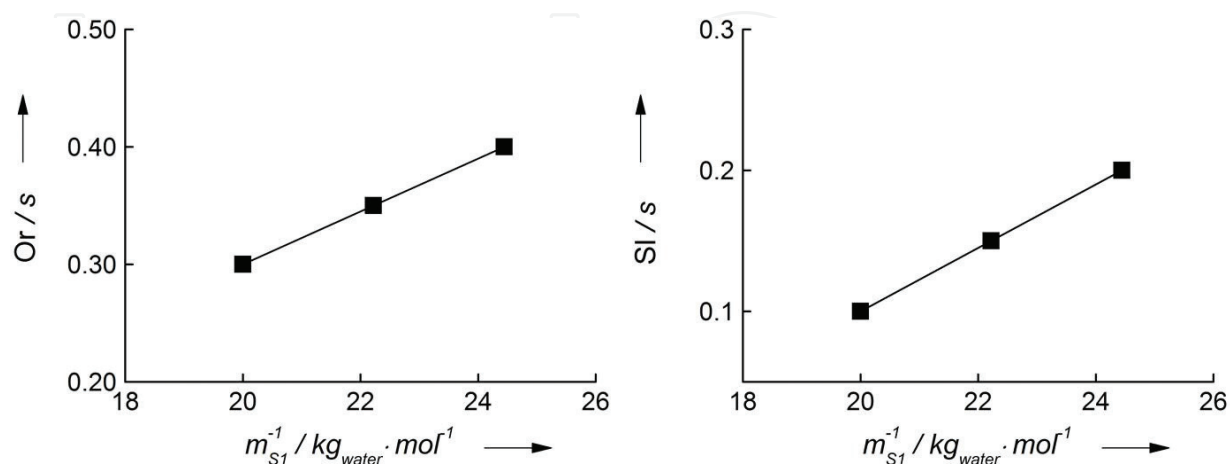


**Figure 5.** Exemplary *secondary plot* for  $Or^{prim}$  (left) and  $SI^{prim}$  (right) over the reciprocal pseudo-constant molalities of  $m_{S1}^{-1}$  derived from the *primary plot* given in **Figure 4**.

$SI_{SI}^{sec}$ ,  $Or_{SI}^{sec}$ ,  $SI_{Or}^{sec}$  and  $Or_{Or}^{sec}$  obtained from the *secondary plots* are defined according to Eqs. (20)–(23):

$$SI_{SI}^{sec} = \frac{K_{iS1}^{obs} \cdot K_{MS2}^{obs}}{k_{cat}} \quad (20)$$

$$Or_{SI}^{sec} = \frac{K_{MS1}^{obs}}{k_{cat}} \quad (21)$$

$$SI_{Or}^{sec} = \frac{K_{MS2}^{obs}}{k_{cat}} \quad (22)$$

$$Or_{Or}^{sec} = \frac{1}{k_{cat}} \quad (23)$$

The relations shown in Eqs. (20)–(23) are finally used to determine  $K_{MS1}^{obs}$ ,  $K_{MS2}^{obs}$ ,  $k_{cat}$  and  $K_{iS1}^{obs}$ .

### 3.1.2. Activity-based approach

The determination of activity-based Michaelis constants  $K_{M,S1}^a$  and  $K_{M,S2}^a$  for two-substrate reactions is analogous to pseudo-one-substrate reactions. As for the pseudo-one-substrate reaction, molalities in Eq. (17) are replaced with activities as shown in Eq. (24):

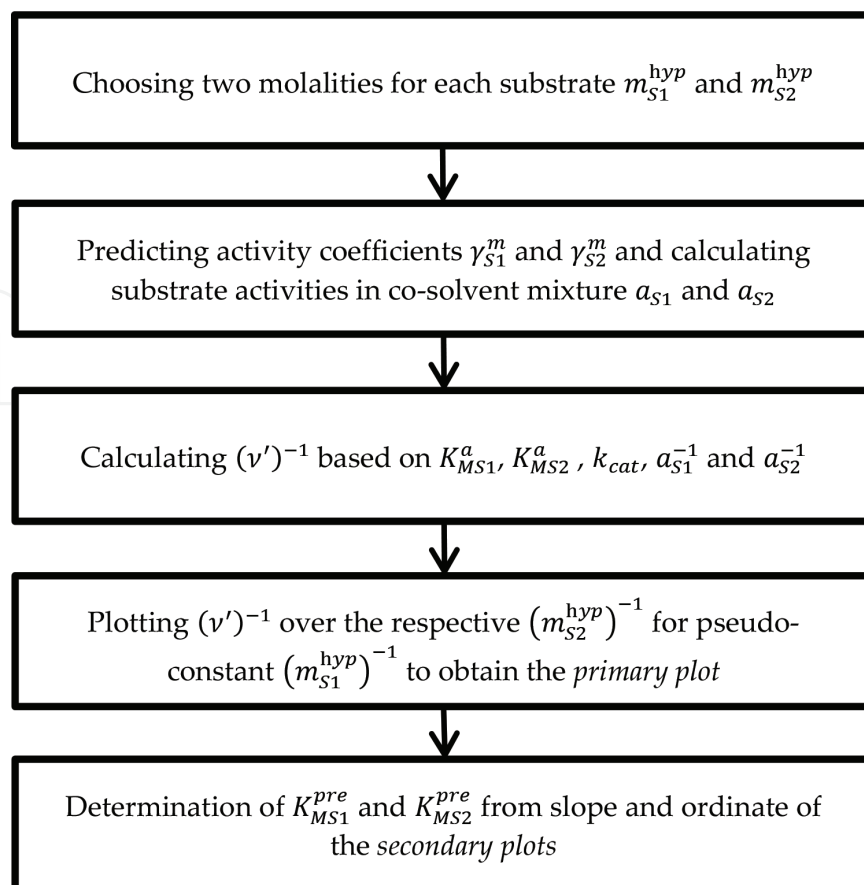
$$\frac{1}{\underbrace{v'}_y} = \underbrace{\left( \frac{K_{iS1}^a \cdot K_{M,S2}^a}{k_{cat} \cdot a_{S2}} + \frac{K_{MS1}^a}{k_{cat}} \right)}_m \cdot \underbrace{\frac{1}{a_{S1}}}_x + \underbrace{\left( \frac{K_{MS2}^a}{k_{cat} \cdot a_{S2}} + \frac{1}{k_{cat}} \right)}_b \quad (24)$$

From Eq. (24), a *primary plot* is created as described in Section 3.1.1 in which  $(v')^{-1}$  is plotted over  $a_{S1}^{-1}$ . Afterwards, the two *secondary plots* are created by plotting the  $Or^{prim}$  and  $SI^{prim}$  of the *primary plot* over  $a_{S1}^{-1}$  to finally obtain the activity-based kinetic constants  $K_{iS1}^a$ ,  $K_{MS1}^a$  and  $K_{MS2}^a$  as described for the concentration-based approach in Section 3.1.1.

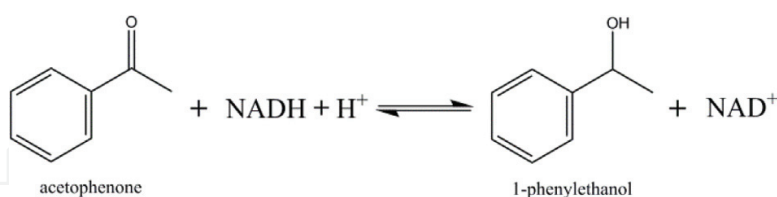
Predictions for the co-solvent influence on  $K_{MS1}^{obs}$  and  $K_{MS2}^{obs}$  are performed in analogy to pseudo-one-substrate reactions: Two molalities of S1  $m_{S1}^{hyp}$  for two molalities of S2  $m_{S2}^{hyp}$  have to be chosen; then, the required activity coefficients have to be predicted in order to create a predicted *primary plot*; the *secondary plots* are then constructed by plotting  $Or^{prim}$  and  $SI^{prim}$  over the chosen reciprocal molalities  $(m_{S2}^{hyp})^{-1}$ . In a final step, the predicted Michaelis constants  $K_{MS1}^{pre}$  and  $K_{MS2}^{pre}$  are obtained from the *secondary plots*. The prediction process is illustrated in **Scheme 3**.

## 3.2. Materials and methods

In this work, the reduction of acetophenone by two different enzymes, ADH 270 and ADH 200, was investigated as model reaction for a two-substrate reaction. The reaction scheme is given in **Scheme 4**. Kinetic data for the ADH 270 were taken from [23].



**Scheme 3.** Steps for the prediction of the concentration-based Michaelis constants  $K_{MS1}^{pre}$  and  $K_{MS2}^{pre}$  under the influence of co-solvents. Predictions are based on the determined activity-based Michaelis constants  $K_{MS1}^a$  and  $K_{MS2}^a$ .



**Scheme 4.** Reaction scheme for the reduction of acetophenone to 1-phenylethanol with the co-substrate nicotinamide adenine dinucleotide in its protonated form (NADH+H<sup>+</sup>) and its deprotonated form (NAD<sup>+</sup>) catalysed by two different genetically modified alcohol dehydrogenases recombinant from *E. coli* (evo-1.1.270; evo-1.1.200).

### 3.2.1. Chemicals

2-[4-(2-hydroxyethyl)piperazin-1-yl]ethanesulfonic acid (HEPES) and polyethylene glycol 6000 (PEG 6000) were purchased from VWR. Acetophenone (ACP) and NADH were purchased from Sigma Aldrich. Sodium hydroxide was purchased from Bernd Kraft GmbH. The genetically modified enzyme alcohol dehydrogenase 200 (evo-1.1.20) expressed recombinant in *E. coli* was purchased from Evoxx. All chemicals were used without further purification, and all samples were prepared using Millipore water from the Milli-Q provided by Merck Millipore as stated in the chemical provenance (Table 5). Kinetic results using the genetically modified enzymes alcohol dehydrogenase 270 (evo-1.1.270) were taken from [23].

Compound	Purity	CAS	Supplier
2-[4-(2-hydroxyethyl)piperazin-1-yl]ethanesulfonic acid (HEPES)	>99%	7365-459	VWR
Polyethylene glycol 6000	—	25322-68-3	VWR
Acetophenone (ACP)	>99%	98-86-2	S
NADH	>97%	606-68-8	S
Sodium hydroxide	>98%	1310-73-2	BK
Alcohol dehydrogenase 200 (evo-1.1.200)	30%	evo-1.1.200	E

S = Sigma Aldrich Chemie GmbH; VWR = VWR International GmbH; BK = Bernd Kraft GmbH; E = Evoxx technologies GmbH.

**Table 5.** Chemical provenance table for the components measured in this work.

### 3.2.2. Kinetic assays

Reactions were carried out in an HEPES buffer (0.1 mol/kg<sub>water</sub>) at pH 7. The pH of the buffer and each sample was measured using a pH electrode from Mettler Toledo (uncertainty  $\pm 0.01$ ) and adjusted with sodium hydroxide when required. For measurements of the co-solvent influence, 17 wt.% of PEG 6000 was added to the buffer. In the first step, the substrate solutions of ACP were prepared in equal number to the different NADH concentrations measured. Buffer was added to 5 ml Eppendorf cups, and ACP was added gravimetrically afterwards using the XS analytical balance provided by Mettler Toledo (uncertainty  $\pm 0.01$  mg). Eppendorf cups were filled to the maximum capacity in order to decrease losses of ACP to the vapour phase. The ACP stock solutions were preheated in an Eppendorf ThermoMixer C at 25°C. ACP concentrations of the neat reaction were 20, 30 and 40 mmol/kg<sub>water</sub> and 60, 80 and 100 mmol/kg<sub>water</sub> for the PEG 6000 measurements, respectively. NADH was added gravimetrically to the ACP solution after preheating. Each sample was prepared directly before measurements due to reported long-term instability of NADH in solution [32]. NADH concentrations were chosen to be 0.15, 0.2, 0.25, 0.3, 0.35 and 0.4 mmol/kg<sub>water</sub>. The enzyme stock solution was prepared by gravimetrically adding 1 wt.% of enzyme to 2 ml of buffer with direct storage on ice for the period of all measurements to ensure enzyme stability and activity. To initiate the kinetic measurements, 20 mg of the enzyme solution was transferred into a quartz cuvette SUPRASIL TYP 114-QS from Helma Analytics which was preheated to 25°C while being placed in an Eppendorf Biospectrometer. After addition of 1 g of the substrate solution containing ACP and NADH, the measurement of the extinction over time at 340 nm wavelength was initiated.

## 3.3. Results and discussion

### 3.3.1. ADH 270

In a first step, the *primary plot* for the ACP reduction catalysed by ADH 270 was determined under neat conditions. For this,  $(v')^{-1}$  is plotted over  $m_{\text{NADH}}^{-1}$  for pseudo-constant  $m_{\text{ACP}}$  levels of 20, 30 and 40 mmol/kg<sub>water</sub> in **Figure 6**.

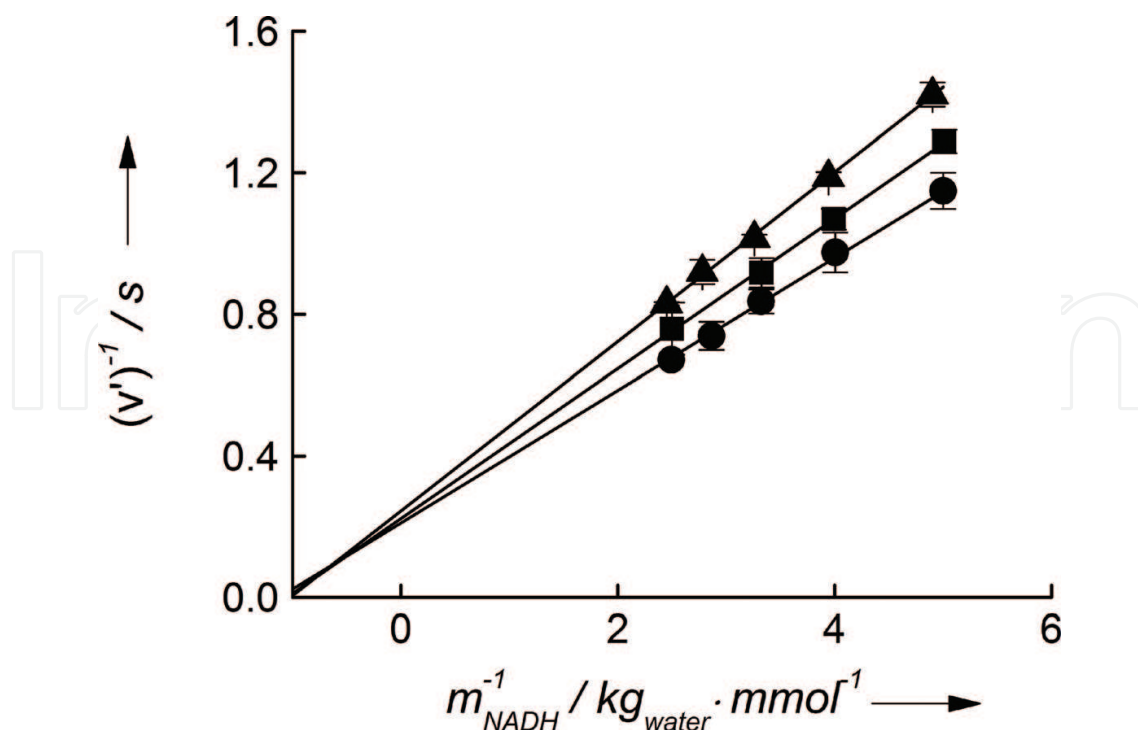


**Figure 6.** Primary plot based on Eq. (17) for the ACP reduction catalysed by ADH 270 under neat conditions at  $T = 25^{\circ}C$ ,  $p = 1$  bar and  $pH = 7$  in HEPES buffer [23]. The reciprocal turnover frequency normalised to the total enzyme concentration  $(v')^{-1}$  is plotted over the reciprocal initial molality of NADH  $m_{NADH}^{-1}$  for ACP molalities of 20 (triangles), 30 (squares) and 40  $mmol/kg_{water}$  (circles). Lines represent the respective fit lines required for further data analysis.

A linear correlation of  $(v')^{-1}$  over  $m_{NADH}^{-1}$  can be observed from **Figure 6**. As described in Section 3.1.1, this correlation is used for the creation of the *secondary plots* shown in **Figure 7**.

**Figure 7** shows the required linear correlation between  $Or^{prim}$  and  $Sl^{prim}$  over  $m_{ACP}^{-1}$  required for the determination of the Michaelis constants  $K_{M,NADH}^{obs}$  and  $K_{M,ACP}^{obs}$  according to Eqs. (20)–(23). Applying the relations given in Eqs. (20)–(23), the Michaelis constant of NADH

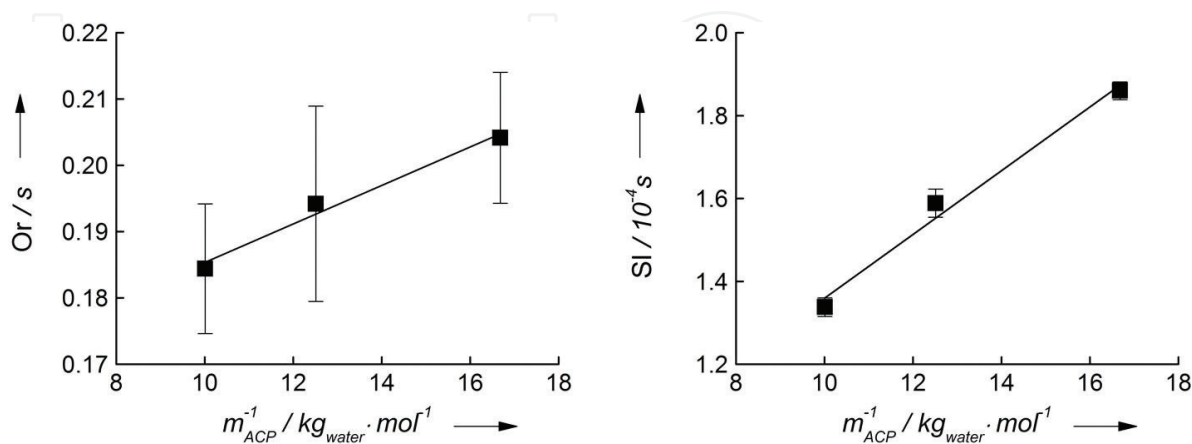


**Figure 7.** Secondary plots based on Eqs. (18) and (19) for the ACP reduction catalysed by ADH 270 under neat conditions at  $T = 25^{\circ}C$ ,  $p = 1$  bar and  $pH = 7$  in HEPES buffer [23]. Left: Ordinates  $Or^{prim}$  of the fit lines resulting from the primary plot are plotted over the reciprocal initial molality of ACP  $m_{ACP}^{-1}$ . Right: Slopes  $Sl^{prim}$  of the fit lines resulting from the primary plot are plotted over the reciprocal initial molality of ACP  $m_{ACP}^{-1}$ . Lines represent the respective fit lines required for further data analysis.

$K_{M,NADH}^{obs} = 0.37 \pm 0.09 \text{ mmol/kg}_{water}$  and of ACP  $K_{M,ACP}^{obs} = 18.56 \pm 3.23 \text{ mmol/kg}_{water}$  were determined [23]. Afterwards, activity coefficients for NADH and ACP were predicted for the respective molalities; these ePC-SAFT predictions are based on the pure-component and binary interaction parameters listed in **Tables 6** and **7**. Based on the activities of NADH  $a_{NADH}$  and ACP  $a_{ACP}$ , the respective *primary* and *secondary plots* were created.

In analogy to the concentration-based approach, activity-based Michaelis constants were determined (Section 3.1.2) to be  $K_{M,NADH}^a = 5.649 \cdot 10^{-8}$  and  $K_{M,ACP}^a = 0.640$ . As can be seen, activity-based Michaelis constants can be completely different from their concentration-based pendants; they even do not have any unit due to the definition of the activity as shown in Eq. (12). In the next step, a prediction of the co-solvent influence of 17 wt.% of PEG 6000 on  $K_{M,ACP}^{obs}$  and  $K_{M,NADH}^{obs}$  was performed as described in Section 3.2.1. These predictions were compared to experimental results given in **Figure 8** and **Table 8**.

As can be seen from **Figure 8** and **Table 8**, predictions of the co-solvent influence of 17 wt.% of PEG on  $K_{M,NADH}^{obs}$  and  $K_{M,ACP}^{obs}$  of the ACP reduction catalysed by ADH 270 are in very good agreement with experimental data. Upon addition of 17 wt.% PEG 6000,  $K_{M,NADH}^{obs}$  decreased by a factor of two, while  $K_{M,ACP}^{obs}$  increased by a factor of 2.5. Both trends were predicted

Component	$m_i$ (–)	$\sigma_i$ (Å)	$\frac{u_i}{k_B}$ (K)	$N_i^{assoc}$	$\frac{\epsilon^{A_i B_j}}{k_B}$ (K)	$\kappa^{A_i B_j}$ (–)
Water [29]	1.204	[A]	353.95	1:1	2425.7	0.0451
ACP [4]	3.40	3.65	322.00	1:1	0	0.0451
NADH [33]	27.27	2.21	260.72	8:8	358.2	0.0001
PEG [25]	$M_{PEG} \cdot 0.05$	2.90	204.60	4:4	1799.8	0.020
Na <sup>+</sup> [34]	1	2.82	230	–	–	–
OH <sup>–</sup> [34]	1	2.02	650.00	–	–	–

[A]  $\sigma_i = 2.7927 + 10.11 \cdot \exp(-0.01775 \cdot T) - 1.417 \cdot \exp(0.01146 \cdot T)$ .

**Table 6.** ePC-SAFT pure-component parameters.

Binary pair	$k_{ij}$ (–)
Water-ACP [4]	0.0330
Water-NADH [33]	–0.0585
Water-PEG [25]	[A]
Water-Na <sup>+</sup> [34]	[B]
Water-OH <sup>–</sup> [34]	–0.25
Na <sup>+</sup> -OH <sup>–</sup> [34]	0.649

[A]  $k_{ij}(T) = -0.135 + 0.0023439 \cdot (T[K] - 298.15)$ .  
 [B]  $k_{ij}(T) = 0.00045485 - 0.007981 \cdot (T[K] - 298.15)$ .

**Table 7.** ePC-SAFT binary interaction parameters  $k_{ij}$ .

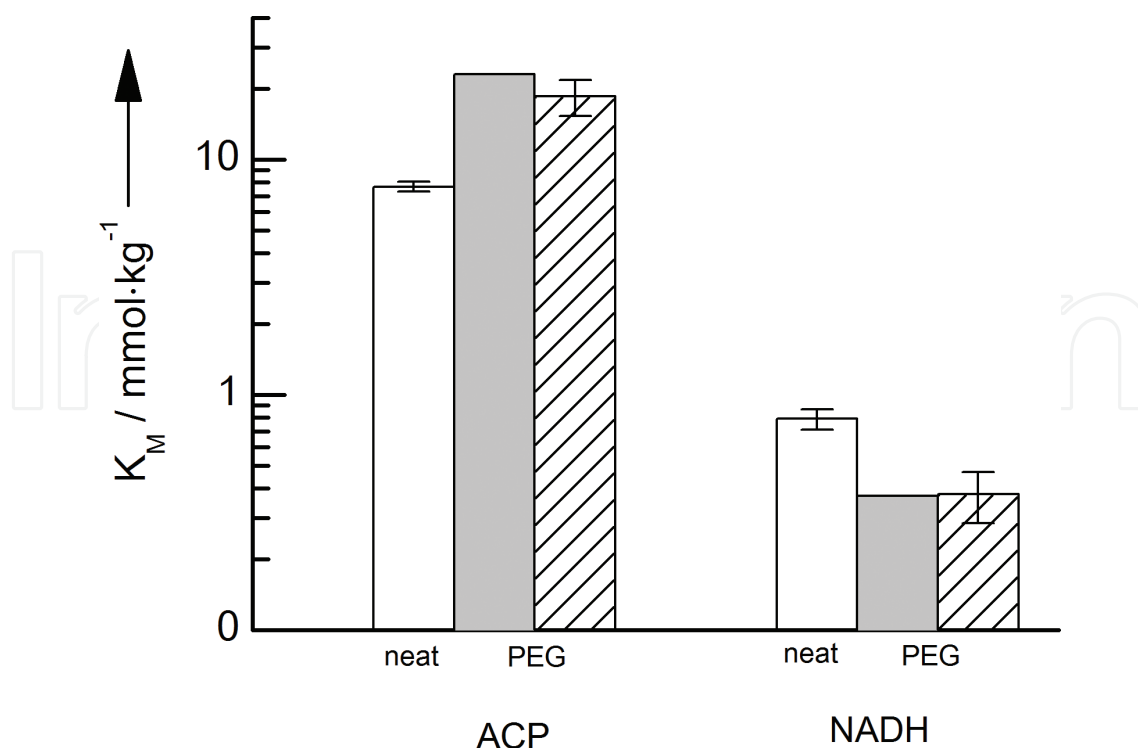


**Figure 8.** Comparison between the experimentally measured Michaelis constants  $K_M^{obs}$  of ACP and NADH under neat reaction conditions (white bars) and under the influence of 17 wt.% PEG 6000 (striped bars) for the reduction of ACP catalysed by ADH 270 at  $T = 25^\circ\text{C}$ ,  $p = 1$  bar and  $\text{pH} = 7$ . The grey bars present the prediction of the respective  $K_M^{pre}$  based on the determined activity-based  $K_M^a$  from the experimental neat data [23]. Required activity coefficients were calculated with ePC-SAFT based on the parameters from **Tables 6** and **7**.

	$K_{M,NADH}^{obs} \left[ \frac{\text{mmol}}{\text{kg}_{\text{water}}} \right]$	$K_{M,NADH}^{pre} \left[ \frac{\text{mmol}}{\text{kg}_{\text{water}}} \right]$	$K_{M,ACP}^{obs} \left[ \frac{\text{mmol}}{\text{kg}_{\text{water}}} \right]$	$K_{M,ACP}^{pre} \left[ \frac{\text{mmol}}{\text{kg}_{\text{water}}} \right]$
Neat	$0.79 \pm 0.08$	—	$7.67 \pm 0.37$	—
17 wt.% PEG 6000	$0.377 \pm 0.09$	0.372	$18.56 \pm 3.23$	23.00

Activity coefficients required for the prediction were calculated with ePC-SAFT based on the parameters from **Tables 6** and **7**.

**Table 8.** Overview of the Michaelis constants under neat reaction conditions and the comparison between predicted  $K_M^{pre}$  and experimentally determined Michaelis constants  $K_M^{obs}$  [23] for the reduction of ACP catalysed by ADH 270 at  $T = 25^\circ\text{C}$ ,  $p = 1$  bar and  $\text{pH} = 7$ .

accurately with ePC-SAFT. This shows that the influence of PEG 6000 on the  $K_M^{obs}$  values is caused by non-covalent molecular interactions between the co-solvent and the substrates instead of co-solvent-enzyme interactions.

### 3.3.2. ADH 200 and comparison to ADH 270

To further validate this approach, the ACP reduction was also investigated with ADH 200 as catalyst. This step is important to support the hypothesis that co-solvent-substrate interactions determine the co-solvent influence on  $K_{M,ACP}^{obs}$  and  $K_{M,NADH}^{obs}$ . However, it becomes obvious from **Table 9** that ADH 200 shows a completely different kinetic profile under neat conditions.

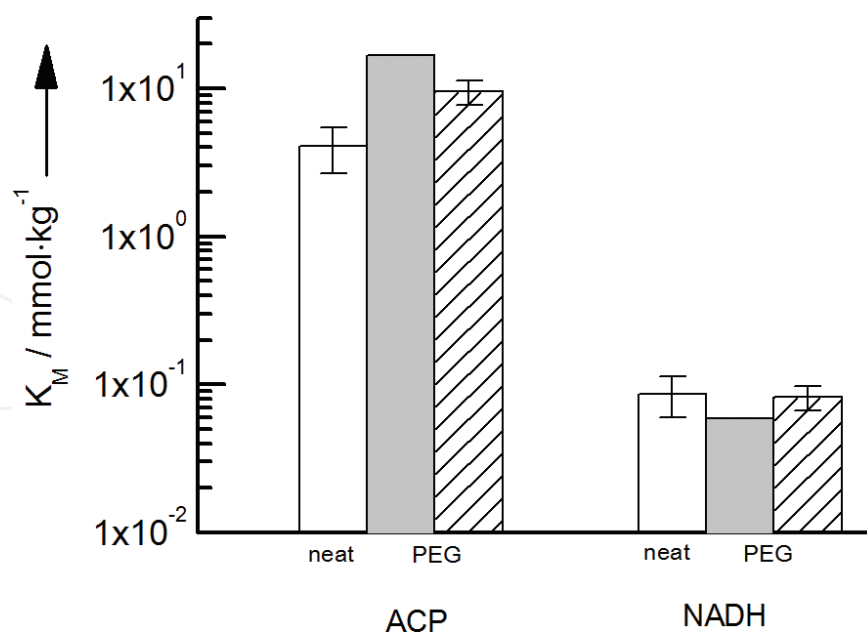


**Figure 9.** Comparison between the experimentally measured Michaelis constants  $K_M^{obs}$  for ACP and NADH from this work under neat reaction conditions (white bars) and under the influence of 17 wt.% PEG 6000 (striped bars) for the reduction of ACP catalysed by ADH 200 at  $T = 25^\circ\text{C}$ ,  $p = 1$  bar and  $\text{pH} = 7$ . The grey bars present the predicted values for  $K_M^{pre}$  based on the determined activity-based  $K_M^a$  from the experimental neat data. Required activity coefficients were predicted with ePC-SAFT based on the parameters from **Tables 6** and **7**.

Enzyme	$K_{M,NADH}^{obs} \left[ \frac{\text{mmol}}{\text{kg}_{\text{water}}} \right]$	$K_{M,NADH}^a [-]$	$K_{M,ACP}^{obs} \left[ \frac{\text{mmol}}{\text{kg}_{\text{water}}} \right]$	$K_{M,ACP}^a [-]$
ADH 270 [23]	$0.79 \pm 0.08$	$5.65 \cdot 10^{-8}$	$7.67 \pm 0.37$	0.640
ADH 200 [this work]	$0.086 \pm 0.027$	$1.16 \cdot 10^{-8}$	$4.08 \pm 1.03$	0.749

**Table 9.** Comparison between the Michaelis constants of NADH and ACP for the reduction of ACP for neat reaction conditions at  $T=25^\circ\text{C}$ ,  $p=1$  bar and  $\text{pH}=7$  in HEPES buffer. Two different enzymes were used as catalyst, ADH 270 and ADH 200. Activity coefficients required for the prediction of  $K_M^a$  were calculated with ePC-SAFT based on the parameters from **Table 6** and **Table 7**.

**Table 9** shows that  $K_{M,NADH}^{obs}$  ( $K_{M,ACP}^{obs}$ ) using ADH 200 are 9 times (2 times) lower than  $K_{M,NADH}^{obs}$  ( $K_{M,ACP}^{obs}$ ) using ADH 270 for identical conditions. Nevertheless, this is an expected behaviour. It can be further observed from **Table 9** that also the activity-based Michaelis constants  $K_{M,NADH}^a$  and  $K_{M,ACP}^a$  are different for ADH 200 and ADH 270 for the ACP reduction at same conditions. The prediction results of the influence of 17 wt.% PEG 6000 on  $K_M^{obs}$  of the reaction catalysed by ADH 200 are given in **Figure 9**.

**Figure 9** shows that ePC-SAFT is able to predict the change of  $K_{M,NADH}^{obs}$  and  $K_{M,ACP}^{obs}$  under the influence of 17 wt.% of PEG 6000 for ADH 200 in good agreement with experimental data. The same ePC-SAFT parameters were used as for the prediction of the same reaction catalysed by ADH 270. This is a further validation of our approach as it shows that predictions are possible independent of the enzyme catalysing the reaction. For both enzymes, ADH 200 and ADH 270, the co-solvent influences on the substrate activities were the key for predicting the change in  $K_M^{obs}$ .

## 4. Conclusion

In this work, it was found that experimental Michaelis constants  $K_M^{obs}$  of a pseudo-one-substrate and a two-substrate reaction were strongly dependent on the co-solvent present in the reaction mixture. This co-solvent effect was assumed to be introduced by the thermodynamic non-ideality caused by molecular interactions. These are expressed as activity coefficients of the substrate(s), which were predicted by the equation of state ePC-SAFT. By accounting for the activity coefficients of the substrate(s), the concentration-based Michaelis constants  $K_M^{obs}$  were expressed as activity-based values  $K_M^a$ . This approach focused on investigating enzyme-independent interactions between co-solvent and the substrate(s) of the reaction; this has the advantage that  $K_M^a$  is a constant value independent of kind or concentration of co-solvent, while the experimentally observed  $K_M^{obs}$  values depend on co-solvent. The availability of  $K_M^a$  then allowed predicting co-solvent-induced changes in  $K_M^{obs}$  and therewith (1) proved the hypothesis that substrate-co-solvent interactions are responsible for changes of  $K_M^{obs}$  upon co-solvent addition and (2) enzyme-co-solvent interactions do not play a role for the observed changes in  $K_M^{obs}$ . Based on these findings, we could suggest that  $K_M^a$  should be considered instead of  $K_M^{obs}$  for investigations of enzyme-catalysed reactions in order to significantly reduce experimental effort and to gain new insight and understanding of the co-solvent-substrate-enzyme interactions present in more complex reaction mixtures, approaching *in cellulo* reaction conditions. We showed the feasibility of this by accurately predicting the influence of co-solvents (e.g., DMSO, urea or TMAO) on the Michaelis constants of a pseudo-one-substrate reaction as well as of a two-substrate ADH reaction. For the latter, the predictions were accurate for two different enzymes (ADH 200 and ADH 270) under investigation. This can be seen as another validation of the hypotheses (1) and (2).

## Acknowledgements

AW and CH gratefully acknowledge the financial support of DAAD (project number 57340264) funded by the Federal Ministry of Education and Research (BMBF). Further, this work was supported by the Cluster of Excellence RESOLV (EXC 1069) funded by the Deutsche Forschungsgemeinschaft (DFG).

## Conflict of interest

The authors declare no conflict of interest. Note that reference [23] is still under second review.

## Author details

Anton Wangler, Mark Jonathan Bunse, Gabriele Sadowski and Christoph Held\*

\*Address all correspondence to: [christoph.held@tu-dortmund.de](mailto:christoph.held@tu-dortmund.de)

Department of Biochemical and Chemical Engineering, Laboratory of Thermodynamics, TU Dortmund University, Dortmund, Germany

## References

- [1] Straathof AJJ, Panke S, Schmid A. The production of fine chemicals by biotransformations. *Current Opinion in Biotechnology*. 2002;**13**(6):548-556
- [2] Carrea G, Riva S. Properties and synthetic applications of enzymes in organic solvents. *Angewandte Chemie International Edition*. 2000;**39**(13):2226-2254
- [3] Schulze B, Wubbolts MG. Biocatalysis for industrial production of fine chemicals. *Current Opinion in Biotechnology*. 1999;**10**(6):609-615
- [4] Voges M et al. Measuring and predicting thermodynamic limitation of an alcohol dehydrogenase reaction. *Industrial & Engineering Chemistry Research*. 2017;**56**(19):5535-5546
- [5] Voges M et al. Thermodynamics of the alanine aminotransferase reaction. *Fluid Phase Equilibria*. 2016;**422**:87-98
- [6] Wangler A et al. Standard Gibbs energy of metabolic reactions: III the 3-phosphoglycerate kinase reaction. *ACS Omega*. 2018;**3**(2):1783-1790
- [7] Wangler A et al. Co-solvent effects on reaction rate and reaction equilibrium of an enzymatic peptide hydrolysis. *Physical Chemistry Chemical Physics*. 2018;**20**(16):11317-11326
- [8] Bisswanger H. *Enzymkinetik: Theorie und Methoden*. 3rd ed. Weinheim: Wiley-VCH; 2000
- [9] Segel IH. *Enzyme Kinetics: Behavior and Analysis of Rapid Equilibrium and Steady State Enzyme Systems*. New York: Wiley; 1975
- [10] Grosch J-H et al. Thermodynamic activity-based intrinsic enzyme kinetic sheds light on enzyme-solvent interactions. *Biotechnology Progress*. 2017;**33**(1):96-103
- [11] Smith RR, Canady WJ. Solvation effects upon the thermodynamic substrate activity; correlation with the kinetics of enzyme catalyzed reactions. II. More complex interactions of alpha-chymotrypsin with dioxane and acetone which are also competitive inhibitors. *Biophysical Chemistry*. 1992;**43**(2):189-195

- [12] Verma SK, Ghosh KK. Catalytic activity of enzyme in water/organic cosolvent mixtures for the hydrolysis of p-nitrophenyl acetate and p-nitrophenyl benzoate. *Indian Journal of Chemistry*. 2010;**49**:1041-1046
- [13] Ereemeev NL. Interaction of  $\alpha$ -chymotrypsin with dimethyl sulfoxide: A change of substrate could "change" the interaction mechanism. *Russian Journal of Bioorganic Chemistry*. 2003;**29**(5):434-440
- [14] Pleiss J. Thermodynamic activity-based interpretation of enzyme kinetics. *Trends in Biotechnology*. 2017;**35**(5):379-382
- [15] Pleiss J. Thermodynamic activity-based progress curve analysis in enzyme kinetics. *Trends in Biotechnology*. 2018;**36**(3):234-238
- [16] Chen CC, Song Y. Generalized electrolyte-NRTL model for mixed-solvent electrolyte systems. *AIChE Journal*. 2004;**50**(8):1928-1941
- [17] Fredenslund A, Jones Russell L, Prausnitz John M. Group-contribution estimation of activity coefficients in nonideal liquid mixtures. *AIChE Journal*. 1975;**21**(6):1086-1099
- [18] Cameretti LF, Sadowski G, Mollerup JM. Modeling of aqueous electrolyte solutions with perturbed-chain statistical associated fluid theory. *Industrial & Engineering Chemistry Research*. 2005;**44**(9):3355-3362
- [19] Dowd JE, Riggs DS. A comparison of estimates of Michaelis-Menten kinetic constants from various linear transformations. *Journal of Biological Chemistry*. 1965;**240**(2):863-869
- [20] Held C, Cameretti LF, Sadowski G. Modeling aqueous electrolyte solutions: Part 1. Fully dissociated electrolytes. *Fluid Phase Equilibria*. 2008;**270**(1-2):87-96
- [21] Held C, Cameretti LF, Sadowski G. Measuring and modeling activity coefficients in aqueous amino-acid solutions. *Industrial & Engineering Chemistry Research*. 2011;**50**(1):131-141
- [22] Held C, Sadowski G. Thermodynamics of bioreactions. *Annual Review of Chemical and Biomolecular Engineering*. 2016;**7**(1):395-414
- [23] Wangler A et al. Prediction and experimental validation of co-solvent influence on Michaelis constants: A thermodynamic activity-based approach. *Chemistry – A European Journal*. 2018. <https://doi.org/10.1002/chem.201803573>
- [24] Prudic A, Ji Y, Sadowski G. Thermodynamic phase behavior of API/polymer solid dispersions. *Molecular Pharmaceutics*. 2014;**11**(7):2294-2304
- [25] Reschke T, Brandenbusch C, Sadowski G. Modeling aqueous two-phase systems: I. Polyethylene glycol and inorganic salts as ATPS former. *Fluid Phase Equilibria*. 2014;**368** (Supplement C):91-103
- [26] Gross J, Sadowski G. Application of perturbation theory to a hard-chain reference fluid: An equation of state for square-well chains. *Fluid Phase Equilibria*. 2000;**168**(2):183-199
- [27] Rosin C et al. Combined effects of temperature, pressure, and co-solvents on the polymerization kinetics of actin. *ChemPhysChem*. 2015;**16**(7):1379-1385

- [28] Bugnon P et al. High-pressure stopped-flow spectrometer for kinetic studies of fast reactions by absorbance and fluorescence detection. *Analytical Chemistry*. 1996;**68**(17):3045-3049
- [29] Fuchs D et al. Solubility of amino acids: Influence of the pH value and the addition of alcoholic cosolvents on aqueous solubility. *Industrial & Engineering Chemistry Research*. 2006;**45**(19):6578-6584
- [30] Held C, Sadowski G. Compatible solutes: Thermodynamic properties relevant for effective protection against osmotic stress. *Fluid Phase Equilibria*. 2016;**407**:224-235
- [31] Kuby SA. *A Study of Enzymes*. Vol. 2. Boca Raton: CRC Press; 1990
- [32] Gallati H. Stabilisierung des reduzierten  $\beta$ -nicotinamid-adenin-dinucleotid in einem organischen Lösungsmittel. *Clinical Chemistry and Laboratory Medicine*. 1976;**14**(1-12):9-14
- [33] Wangler A et al. Predicting the high concentration co-solvent influence on the reaction equilibria of the ADH-catalyzed reduction of acetophenone. *Journal of Chemical Thermodynamics*. 2019;**128**:275-282
- [34] Held C et al. ePC-SAFT revised. *Chemical Engineering Research and Design*. 2014;**92**(12):2884-2897

